Journal of Hydrology: Regional Studies 30 (2020) 100693

Contents lists available at ScienceDirect

Journal of Hydrology: Regional Studies

journal homepage: www.elsevier.com/locate/ejrh

An integrated approach to estimate the mixing ratios in a karst system under different hydrogeological conditions

Ahmad Behrouj-Peely[a], Zargam Mohammadi[a,*], Laura Scheiber[b], Enric Vázquez-Suñé[b]

[a] Department of Earth Sciences, Shiraz University, 7146713565, Shiraz, Iran
[b] Institute of Environmental Assessment and Water Research (IDAEA), Hydrogeology Group (UPC-CSIC), CSIC, c/ Jordi Girona 18-26, 08034, Barcelona, Spain

ARTICLE INFO

Keywords:
Mixing modeling
Hydrogeology
Karst
Leakage
Seymareh Dam

ABSTRACT

Study region: The karst system of the Syemareh Dam site with the reservoir capacity of 3.2 bm^3, located in the Zagros fold belt, southwestern of Iran, was studied under two conditions: before and after the reservoir impoundment as pre-reservoir and post-reservoir conditions, respectively.
Study focus: Despite a mixing of several water resources including the dam reservoir contributed to the flow rate of the downstream springs, the number of end-members was still unknown and their mixing ratio was unquantified. In this study, firstly a statistical approach (e.g. loading plot and matrix plot) was utilized to identify possible chemical reactions. Then, End Member Mixing Analysis (EMMA) was used to determine the number of end members. Lastly, the MIX code was utilized to quantify the mixing ratios. Three scenarios (i.e. assuming three, four and five end members) were compared to find a reliable mixing model based on the best match between the observed and estimated values of species concentration. In order to improve the calibration of the reliable mixing model, the species concentrations were corrected by deduction of the effect of plausible chemical reactions.
New hydrological insights for the region: The five end-members mixing model consisted of three aquifers, deep groundwater, and the reservoir was suggested as the dominant mixing process. Leakage from the reservoir as an end member was quantified by calculating the mixing ratio of the reservoir through mixing modeling for the first time.

* Corresponding author.
E-mail addresses: behrouj.a@gmail.com (A. Behrouj-Peely), zmohammadi@shirazu.ac.ir (Z. Mohammadi), laura.scheiber@idaea.csic.es (L. Scheiber), enric.vazquez@idaea.csic.es (E. Vázquez-Suñé).

https://doi.org/10.1016/j.ejrh.2020.100693
Received 27 November 2019; Received in revised form 24 March 2020; Accepted 22 April 2020

Nomenclature

Formation

As	Asmari
Gs	Gachsaran
Bk	Bakhtiari
Q	Quarternary sediments

Aquifer

RRA	Right Ravandi aquifer
LRA	Left Ravandi aquifer
GFA	Gachsaran formation aquifer
DG	Deep groundwater

Reservoir

R	Reservoir

Sample

G#B#	Drianage borehole in gallery
LOW#	Observation well of LRA
ROW#	Observation Well of RRA
LSP#	Spring of LRA
RSP#	Spring of RRA
GSP#	Spring of GFA
F	Dam foundation (DG)

1. Introduction

Karst regions represent 7–12 % of the Earth's continental area (Hartmann et al., 2014), in particular, 11 % of Iran's land surface covered by karst limestone (Raeisi and Kowsar, 1997). Large fractures and conduits are the main pathways of groundwater flow in karst aquifers, which cause rapid response to hydrological stresses such as heavy rainfall events and impoundment of dam reservoirs. In addition, man-made stresses such as elevated water pressure by a dam reservoir provides favorable conditions for leakage through karst features which potentially change the hydrogeological setting of the downstream aquifers (Mohammadi et al., 2007a, b; Battaglia et al., 2016; Behrouj et al., 2018; Milanovic, 2018). Increasing discharge at downstream springs and groundwater level as well as variations of hydrochemical composition (Contreras and Hernandez, 2013) are indications of leakage and probably mixing of dam reservoir water with surrounding aquifers. Leakage from dam sites has been reported in numerous dams in karst areas over the world (see for example Milanovic, 2018). A few conventional methods such as geophysical and tracer tests (Boleve et al., 2011), a combination of geological and hydrogeological techniques (Kamble et al., 2014) and numerical modeling (Cheshomi et al., 2014) were utilized to evaluate the leakage amount through dam sites. However, no studies have applied mixing modeling to calculate the reservoir leakage.

In order to quantify the contribution (i.e., mixing ratio) of a dam reservoir in the surrounding aquifers, mixing modeling is a potential approach. Although mixing models have not been particularly used to assess the leakage from a dam site, they have been implemented to determine the age distribution of groundwater (Jurgens et al., 2014), to assess the mechanisms that control stream water chemistry (Katsuyama et al., 2001), to quantify the chemical processes that affect the organic pollutants in an urban aquifer (Jurado et al., 2015), to locate the water inrush in mining industry (Gu et al., 2017), and to quantify the proportion of different water sources in mining (Scheiber et al., 2018), amongst others.

Mixing process defines interaction between two or more sources of water as end-members. Calculation of mixing ratio usually consists of several steps which mainly start by distinguishing end-members followed by mixing modeling. End member mixing analysis (EMMA) has been widely used to identify the number of end-members (Hooper et al., 1990; Christophersen et al., 1990; Hooper, 2003; Vázquez-suñé et al., 2010; Tubau et al., 2014; Pelizardi et al., 2017). EMMA utilizes Principle Component Analysis (PCA) as a multivariate statistical method to find the minimum number of end-members (Christophersen and Hooper, 1992; Mohammadi, 2009; Valder et al., 2012; Chen et al., 2014; Sun and Gui, 2015).

Following the delineation of end-members, a mixing model implemented to quantify the mixing ratios. Conventional mixing models are handled based on some common approaches such as linear mixing and least square. The linear mixing model of n end-members, considering continuity and solute and water mass balance, assumes linear contribution of the end-members to the mixed samples based on the following equations (Carrera et al., 2004):

$$X_1 Q_1 + X_2 Q_2 + ...+X_n Q_n = Y_o Q_o \tag{1}$$

$$Q_1 + Q_2 + ...+Q_n = Q_o \tag{2}$$

Where X_1 to X_n are the concentrations of inflow waters (i.e., end-members), Q_1 to Q_n are the corresponding rates, Y_o is the concentration of outflow water (i.e., mixed water) and Q_o is its rate. By dividing 1 and 2 by Q_o and defining δ as the mixing ratio:

$$X_1 \delta_1 + X_2 \delta_2 + ...+X_n \delta_n = Y_o \tag{3}$$

$$\sum_{i=1}^{i=n} \delta_i = 1 \tag{4}$$

On the other hand, the following equation was introduced for computation of mixing ratio based on least squares and is a general form of Eq. (1) (Carrera et al., 2004):

$$y_{ps} = \sum_{e=1}^{ne} \delta_{ps} x_{es} + \varepsilon_{ps} \tag{5}$$

where y_{ps} and x_{es} are the concentrations of species s in sample p and end-member e, respectively, δ_{ps} is the mixing ratio of end-member e in mixture p, and ε_{ps} is an error which might arise from measurements.

The aforementioned methods assume that the composition of end-members, despite reality, is well-known. Joerin et al. (2002) applied Monte Carlo analysis to specify the uncertainty of a three-end-member mixing model. Rueedi et al. (2005) has presented a statistical multi-parameter procedure to calculate mixing ratios and their uncertainties using a set of chemical and isotopic parameters. Carrera et al. (2004) has presented an algorithm to quantify the mixing ratios using a maximum likelihood method considering this fact that the composition of end-members is not well-known. The following likelihood equation has to be maximized:

$$L_p = \exp\left[-\frac{1}{2}(y_p - F\delta_p)^t A_p^{-1}(y_p - F\delta_p)\right] \tag{6}$$

subject to $\delta_p^t l_{ne} = 1$ where δ_p is the vector of mixing ratios, l_{ne} is a one-dimensional vector of l's, y_p is the vector of all species measured in the pth sample, A_p is covariance matrix of them, and $F = \{x_{es}\}$ is a matrix of all chemical analyses of end-members. The algorithm

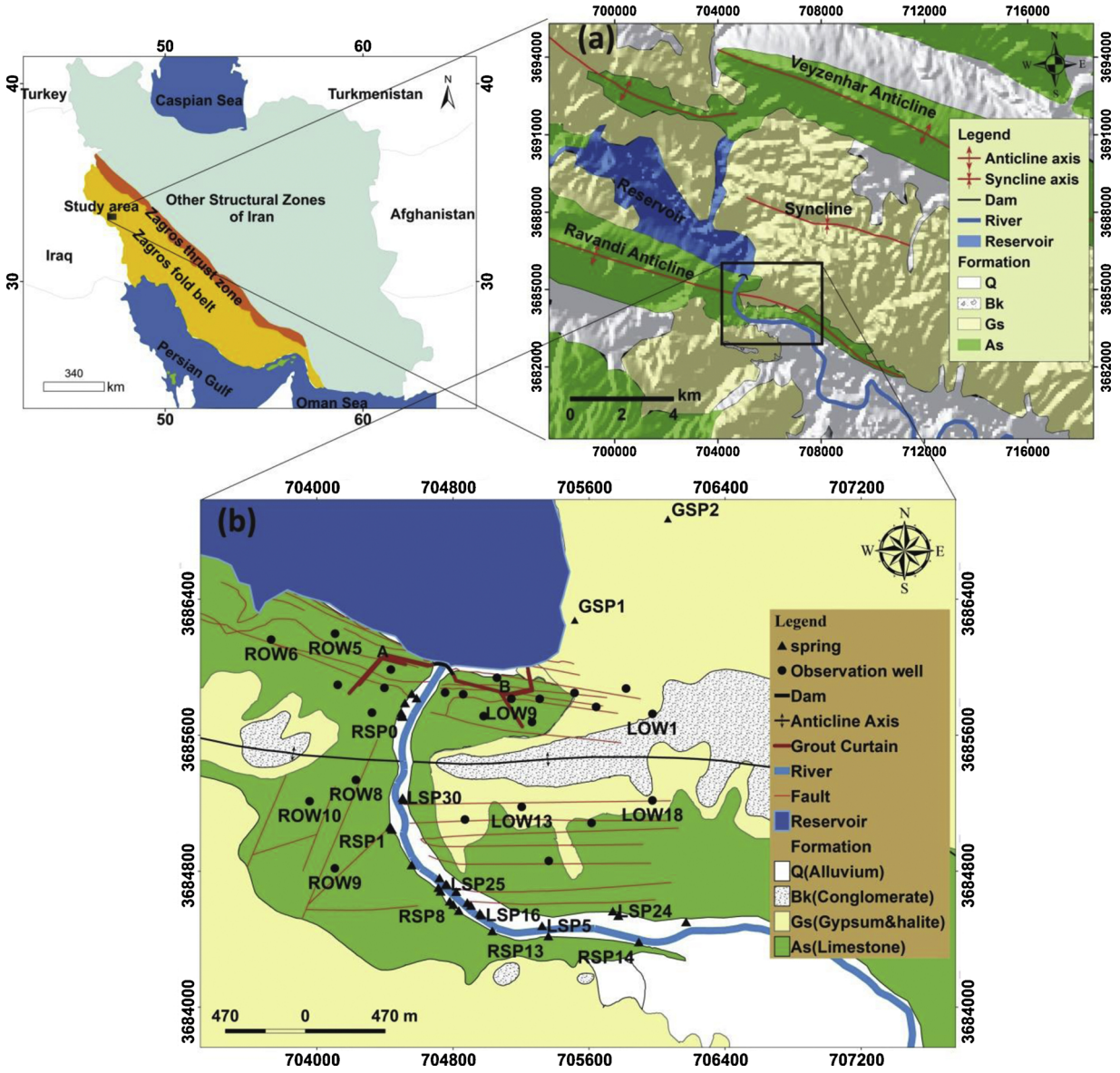

Fig. 1. a) Regional geological map and b) the sampling sites (GSP: Gachsaran formation aquifer spring, LSP and RSP: springs at the Left and Right Ravandi aquifers, respectively, LOW and ROW: observation wells In the Left and Right Ravandi aquifers, respectively.

has been named the Mix code and applied in several studies (Vázquez-suñé et al., 2010; Tubau et al., 2014; Jurado et al., 2015; Scheiber et al., 2018).

To run mixing models, geochemical tracers can be used to quantify mixing ratios (Crandall et al., 1999). In a two end-members mixing model, the proportion of the two unmixed sites in the mixed site is easy to be calculated by measuring the concentration of a conservative ion (e.g. Cl) of the two unmixed sites and of the mixed site using linear mixing or least square approaches. However, mixing modeling for calculating groundwater mixing ratio in three or more end-members needs more data and modeling efforts. For example, $\delta^{18}O$ and Cl − values can be used to identify mixing patterns (Gu et al., 2017). Douglas et al. (2000) has used chemical characteristics and isotopic content of water (i.e. relation between Cl and δ^{18} O) to distinguish groundwater types and to compute mixing ratios.

Despite the wide application of geochemical tracers in mixing modeling, chemical reactions are usually the cause of changes in the geochemistry of groundwater that might induce uncertainty calculating mixing ratios. In order to overcome this uncertainty source, the conservative tracers, which are not being affected by chemical reactions, can be used to improve mixing models (Nakaya et al., 2007; Long and Valder, 2011). The rate of mixing, which can be defined by how different end members contribute, controls the amount of reactants resulting in products (De Simoni et al., 2007). A mixing line drawn between two-end-members can be used to determine whether groundwater has been enriched or depleted with regard to a certain ion based on the situation of the sample related to the mixing line (Ravenscroft and McArthur, 2004). In addition the deviation from this line can be marked to identify geochemical processes (Tubau et al., 2014).

In this research, mixing modeling is implemented in a unique case study where hydrochemical and isotopic characteristics of the aquifers have been changed due to effects of a new end-member (i.e. a dam reservoir named Seymareh). Two hydrogeological conditions including pre-reservoir (i.e. before construction of the dam), and post-reservoir (i.e. after construction of the dam) conditions are considered. Recent studies including dye tracing tests at the Seymareh dam site revealed leakage from the reservoir towards the downstream springs (Behrouj et al., 2018). However, the amount of leakage was unknown in the downstream springs. This study attempts to (1) compare the hydrogeological and hydrochemical characteristics of a karst aquifer under pre-reservoir and post-reservoir conditions, (2) estimate the mixing ratio under different hydrogeological conditions, and (3) evaluate mixing modeling as a practical method to estimate leakage amount based on mixing ratio.

2. Materials and methods

2.1. Site description

The study area including Ravandi anticline is located in the southwestern part of the folded Zagros Mountains (Fig. 1). Geologically, three formations exposed in the study area are, in the order of age, Bakhtiari (Late Pliocene), Gachsaran (Early Miocene), and Asmari (Oligocene-Miocene). Bakhtiari formation (Bk) which is mainly comprised of conglomerate, is the youngest formation and covers some parts of the Ravandi Anticline. Gachsaran formation (Gs), which mainly consists of gypsum and halite, fills the syncline and lies on the top of Asmari formation. The main formation of the Ravandi anticline is the Asmari formation (As) which comprised of limestone (Behrouj et al., 2018).

The Seymareh River, at the elevation of 603 masl (meters above sea level), crosses the Ravandi anticline and provides a tight gorge for construction of the Seymareh dam. The dam has been constructed on the northern flank of the Ravandi anticline (Fig. 1). The reservoir was impounded from 2009 to 2011. The reservoir water level has a measured elevation of 680 masl that has changed the hydrogeological conditions of the study area (e.g. groundwater velocity, hydraulic gradient and mixing processes).

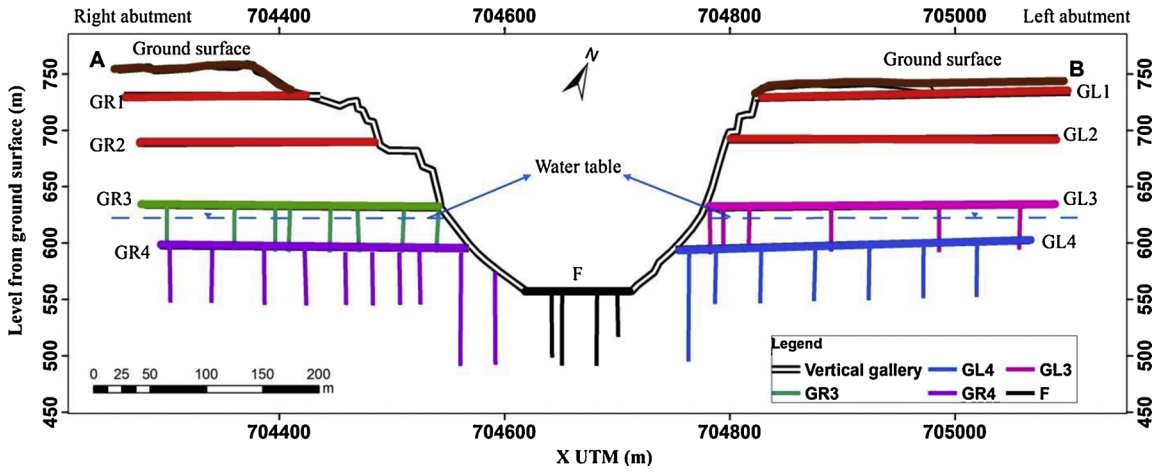

Fig. 2. A cross section along the dam axis with a view from downstream of the dam axis opposite to the river direction (AB line in Fig. 1b) showing the sampling points in the left and right galleries (GL# and GR#, respectively) and in the dam foundation (F).

Two main aquifers including the Ghachsaran formation (GFA), and the Ravandi anticline were identified based on the characteristics of the water resources and outcrops of the Gachsaran and Asmari formations (Behrouj, 2018). GFA is in the northeastern part of the study area. Two permanent springs namely GSP1 and GSP2 with a flow rate of less than 10 L/s discharged GFA in pre-reservoir condition (Fig. 1b). The direction of groundwater flow in this aquifer is towards the Left Ravandi Aquifer (LRA) based on water balance calculations (Bagheri et al., 2006). No springs were observed from this aquifer after reservoir impoundment.

The Ravandi anticline is divided in two sub-aquifers namely Right Ravandi Aquifer (RRA) and Left Ravandi Aquifer (LRA). The general groundwater flow direction is from both flanks of the Ravandi anticline toward the Seymareh River under pre-reservoir and post-reservoir conditions (Behrouj et al., 2018). The minimum and maximum groundwater levels in RRA were about 593 up to 597 masl under pre-reservoir condition and changed to be in the range of 605–658 masl under post-reservoir condition. As for the LRA the minimum and maximum groundwater levels were 594–597 masl under pre-reservoir condition but increased to 603 up to 634 masl under post-reservoir condition. The base of karstification, which can be considered the bottom of the aquifer, according to the drilling data, is at about 470 masl.

There are more than 50 springs that discharge at the Ravandi anticline from both aquifers situated on the banks of the Seymareh River (Fig. 1). LSP24 is the most important spring in terms of flow rate which averages about 432 L/s. The average hydraulic gradient in the Ravandi anticline was computed to be about 0.0005 and 0.015 in before and after the reservoir impoundment, respectively. Consequently the total discharge of the springs has increased from about 2000 L/s to 5000 L/s from pre-reservoir to post-reservoir conditions (Behrouj, 2018).

Availability of hydrochemical, isotopic and dye tracing data in 2006 (Bagheri et al., 2006) before impoundment as the pre-reservoir condition and in 2015 after impoundment as the post-reservoir condition provide sufficient data for differentiating of two distinct hydrogeological conditions. In order to compare the hydrogeology of the study area the measured data in July 2006 and July 2015 were selected as representative of the pre-reservoir and post-reservoir conditions, respectively.

2.2. Sampling and analytical methods

In order to compare the hydrochemical and isotopic characteristics of the aquifers (Gachsaran and Ravandi aquifers) and delineate the endmembers and mixing ratio, two sampling sets (before and after construction of the dam) were selected. Sixty sampling points including 46 springs and 14 observation wells, were sampled before construction of the dam under pre-reservoir conditions in July 2006 (supplementary Table 1). However, the sampling points were increased to 92 including 18 observation wells, 9 drainage boreholes and 21 springs from LRA and 14 observation wells, 8 drainage boreholes and 19 springs from RRA after construction of the dam under post-reservoir condition in July 2015 (supplementary Table 2). The reservoir, a few observation wells, and drainage boreholes in grouting galleries of the dam were sampled in July 2015 only (Figs. 1 and 2). LOW and LSP are abbreviations of the observation wells and springs related to LRA, respectively. For RRA aquifer, ROW and RSP are used to show the observation wells and springs, respectively. The springs emerge close to the river elevation and their outlet elevation ranges from 595 to 603 masl.

Four galleries, numbered from top (G1) with an elevation of about 730 masl to bottom (G4) with an elevation of about 600 masl, were accessible for sampling of groundwater at different depths (Fig. 2). Moreover, a few boreholes in the foundation of the dam drilled to 470 masl, are available for sampling of deep groundwater (Fig. 2). Since, the bottom elevations of G1 and G2 are above the reservoir water level, they are still dry. The samples with abbreviations GR3B and GR4B on the right and GL3B and GL4B on the left belong to G3 and G4, respectively. The samples taken from the right galleries are in RRA and those samples taken from the left galleries are in LRA. The samples from the dam foundation (i.e., deep groundwater) are shown by F.

Major ions (Cl^-, SO_4^{2-}, HCO_3^-, K^+, Na^+, Ca^{2+} and Mg^{2+}) were analyzed at the hydrochemistry laboratory of Shiraz university for all water samples (60 and 92 samples in pre-reservoir and post-reservoir conditions, respectively). Electrical Conductivity (EC), water acidity (pH), and temperature were measured simultaneously in situ. Environmental isotopes (e.g. δ^2 H and δ^{18}O) were analyzed in 32 water samples under pre-reservoir conditions and 20 water samples under post-reservoir conditions at the Environmental Isotope Laboratory, University of Waterloo, Canada. More details of the analysis are presented in supplementary Tables 1 and 2.

2.3. Mixing calculation

The aquifers and the related water resources were studied from a hydrochemical point of view under both pre-reservoir and post-reservoir conditions. In particular, matrix and loading plots, and Piper diagram were constructed to delineate the relationship between the major ions and the most probable chemical reactions. Matrix plots highlight the most meaningful relationship between different species. Loading plots show the importance of ions on the first and second components axes. First and second components are the linear transformation of a few measured variables into two components. Consequently, it is possible to suggest some sources (i.e. end-members) that are the reasons for the plausible chemical reactions.

The elementary number of end-members was determined by PCA. However, the number of end-members was modified to consider the hydrogeological effect caused by the dam reservoir. Hydrochemical and isotopic composition of the water samples collected under both pre-reservoir and post-reservoir conditions were used to make final decisions regarding the end-members and develop a reliable conceptual mixing model.

The MIX Code (Carrera et al., 2004) is used to calculate the mixing ratio of end-members. The model attempts to adjust the measured and calculated concentration of conservative species with an acceptable tolerance value defined by user.

In addition, a few studies have already discussed the chemical reactions for miscalculating the mixing ratios (Tubau et al., 2014; Jurado et al., 2015). The effect of chemical reactions on the mixing model is eliminated by correcting the concentration of species at

sampling sites based on the most probable occurring reactions. An ion concentration (x_c), which can be subtracted or added to the measured concentration depending on the reaction, is defined as:

$$x_c = C_1 \frac{Q_1}{Q_2} \tag{7}$$

Where C_1 is the initial concentration of a sampling site and Q_1 is the corresponding flow rate, x_c is the expected concentration to be added or subtracted from the same site with final corresponding flow rate (Q_2).

The reliability of the end-members can be crosschecked through the calibration process by defining a few reliable scenarios of the end-members. The MIX code is handled for three scenarios including three, four, and five end-members. The mixing model is validated for two data sets (Aug. 2014, and Sep. 2015). Finally, the validated mixing model is used to estimate the mixing ratio of the reservoir as a measure of leakage from the reservoir.

3. Results and discussion

3.1. Hydrochemical characteristics of the samples

Based on the measurements Ca and SO_4 are the dominant ions in RRA and GFA, suggesting a calcium sulfate water type. Na and Cl are the dominant ions in LRA indicating sodium chloride water type under pre-reservoir condition. The SO4 and Ca average concentrations for samples collected under pre-reservoir conditions from GFA were 1184 and 433 ppm, respectively. The average EC of GFA was about 2020 μs/cm. No sampling sites were accessible in GFA under post-reservoir conditions. The average EC increased in the LRA aquifer from 1743 to 2784 μs/cm and in the RRA aquifer from 849 to 2049 μs/cm under pre-reservoir conditions to post-reservoir conditions, respectively.

The average EC of the reservoir is 841 μs/cm and Ca and SO_4 are the dominant ions. The samples from the reservoir show a mean value of 305 and 137 ppm for SO_4 and Ca, respectively. However, the mean concentration of SO_4 and Ca in the RRA aquifer has increased from 244 and 117 ppm to 345 and 142 ppm from pre-reservoir to post-reservoir conditions, respectively. The average concentration of Cl and Na in the LRA aquifer increased from 381 and 191 ppm to 564 and 314 ppm under pre-reservoir to post-reservoir conditions, respectively. The average concentration of HCO_3 in both the LRA aquifer and the RRA aquifer under pre-reservoir condition is about 220 ppm while it is about 205 ppm in GFA. Under post-reservoir condition, the average concentration of

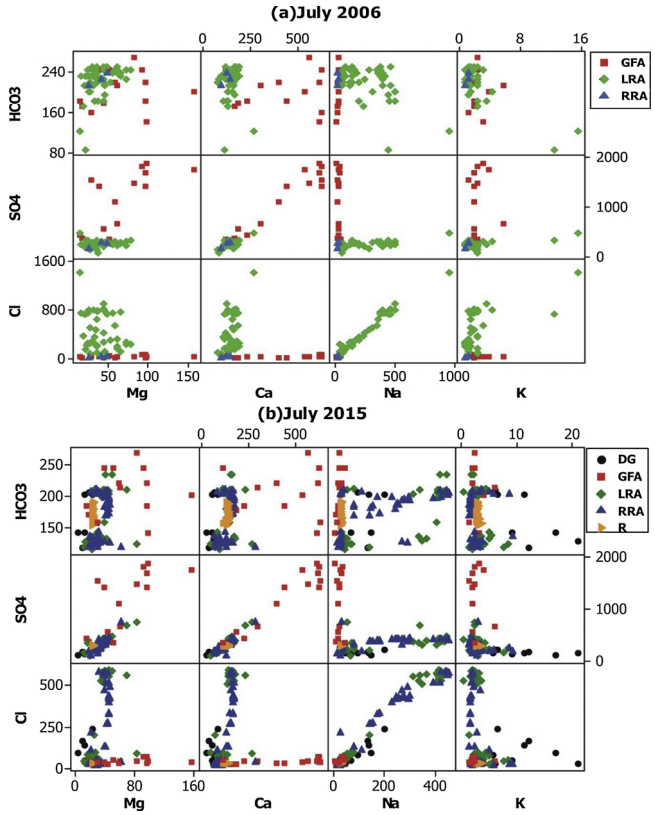

Fig. 3. Matrix diagram for the major ions under (a) pre-reservoir and (b) post-reservoir conditions (RRA: Right Ravandi Aquifer, LRA: Left Ravandi Aquifer, GFA: Gachsaran Formation Aquifer, DG: Deep Groundwater, and R: Reservoir).

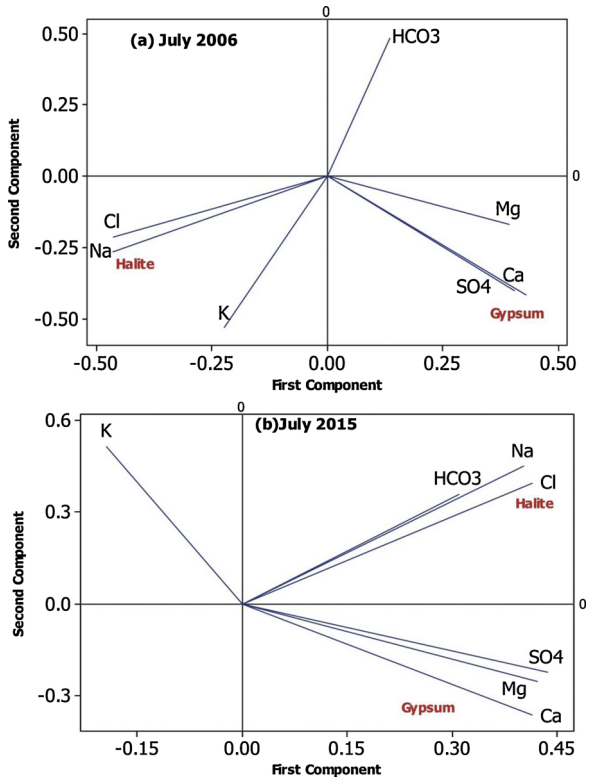

Fig. 4. Loading plot for the major ions under (a) pre-reservoir and (b) post-reservoir conditions.

HCO_3 is about 190, 174, and 168 ppm in the reservoir, LRA aquifer and RRA aquifer, respectively.

Samples from the dam foundation (abbreviated as F in Fig. 2), which has a depth of about 470 masl, are characterized with an EC of about 974 μs/cm and is a Na-Cl water type. A unique aspect of the dam foundation samples is having K^+ concentration of about 11 ppm, which on average, is three times higher than that of other samples which might be an indication of a reaction or even a different source of groundwater.

Based on the matrix plots of the anions versus cations, the most meaningful relationship is found between Cl and Na with Pearson correlation coefficient of 0.985 and 0.986 indicating the solution of halite under both the pre-reservoir and post-reservoir conditions, respectively (Fig. 3). The relationship between Ca variations with SO_4 is also noticeable with Pearson correlation coefficient of 0.975 and 0.98 suggesting the solution of gypsum under both the pre-reservoir and post-reservoir conditions, respectively. However, there is a meaningful match between Mg and SO_4 with Pearson correlation coefficient of 0.81 under post-reservoir conditions that was not found under pre-reservoir conditions with Pearson correlation coefficient of 0.64. Dissolution of halite and gypsum are highlighted in the loading plots (Fig. 4) due to the high loading value of Na and Cl as the first component and Ca, Mg and SO_4 as the first and second components, respectively. Variations of the loading values of Na and Cl under pre-reservoir and post-reservoir conditions suggest increasing halite dissolution under post-reservoir conditions.

3.2. Definition of end-members

In order to define end-members, the water samples from two sets of measurements (July 2006 and July 2015) have initially been plotted on the Piper diagram (Fig. 5). The illustration of the samples on Fig. 5a from pre-reservoir condition reveals that there should be three different groundwater resources including LRA, RRA and GFA before impoundment. The samples on Fig. 5b belong to the post-reservoir conditions plus one sample from GFA under pre-reservoir conditions for comparison. The Piper diagram suggests four end-members based on the distribution of the sampling sites on the diagram representing post-reservoir conditions (Fig. 5b). The end members are suggested, based on the samples from the deep groundwater (DG), LRA, RRA, and GFA. DG is based on the samples from the dam foundations abbreviated as F.

Application of PCA helps identify the samples that exhibit extreme concentrations which can be introduced as end-members (Figs. 6 and 7). Application of PCA for data of pre-reservoir and post-reservoir conditions show that the first two components have eigenvalue more than one but the value of the other components are insignificant for both conditions. PCA suggests at least three end members from three different aquifers namely LRA, RRA and GFA in the pre-reservoir conditions (Fig. 6). For the post-reservoir condition, it was expected that the number of end-members have been increased to four including the dam reservoir. However, PCA shows three end-members, including LRA, GFA and DG under the post-reservoir conditions and there is no evidence for the reservoir

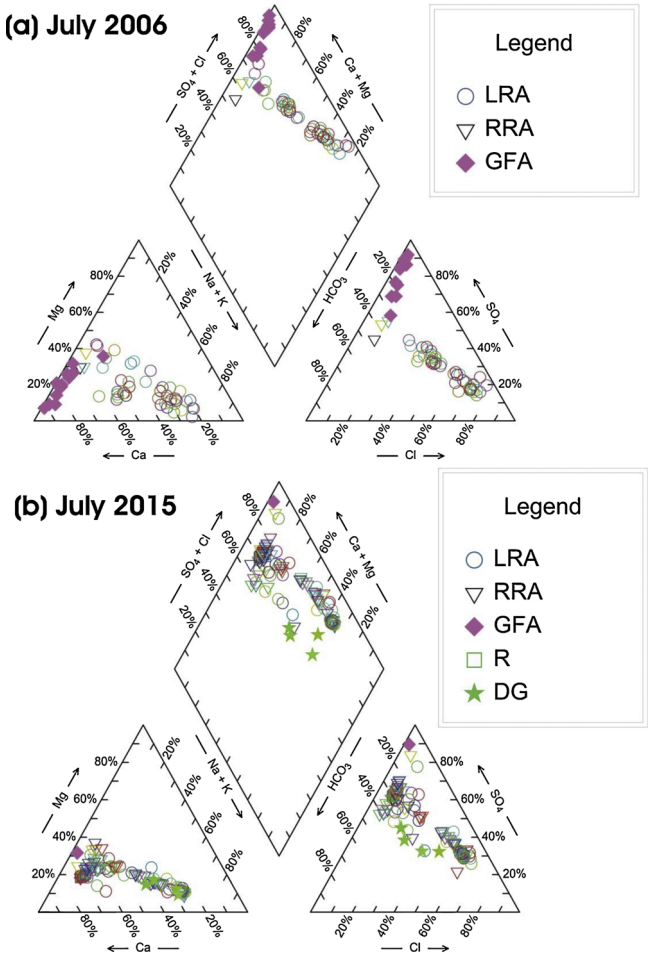

Fig. 5. Piper plot of the sampling sites grouped as the end-members under (a) pre-reservoir and (b) post-reservoir conditions (RRA: Right Ravandi Aquifer, LRA: Left Ravandi Aquifer, GFA: Gachsaran Formation Aquifer, DG: Deep Groundwater, and R: Reservoir).

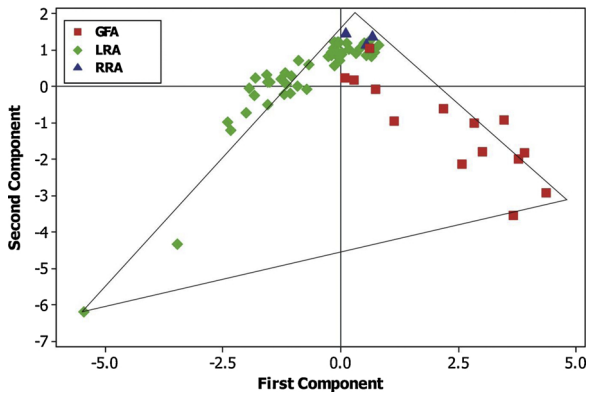

Fig. 6. Score plot of the sampling sites from different aquifers under pre-reservoir condition; the vertices of the triangle are the end-members (RRA: Right Ravandi Aquifer, LRA: Left Ravandi Aquifer, and GFA: Gachsaran Formation Aquifer).

(R) as an end-member (Fig. 7). It seems that the application of the conventional procedure of EMMA method is unable to differentiate the reliable number of end-members due to small differences between the concentration of the species (James and Roulet, 2006).

3.2.1. Modification of the number of end-members

In order to improve the applicability of EMMA, variation of the concentration of Cl as a conservative ion and stable isotopes of δ^2

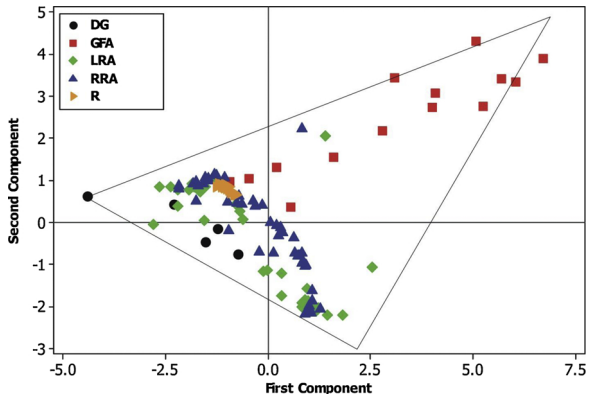

Fig. 7. Score plot of the sampling sites from different aquifers under post-reservoir condition; the vertices of the triangle are the end-members (RRA: Right Ravandi Aquifer, LRA: Left Ravandi Aquifer, GFA: Gachsaran Formation Aquifer, DG: Deep Groundwater, and R: Reservoir).

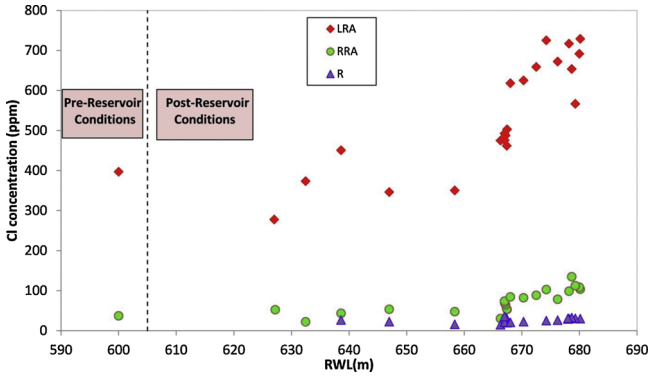

Fig. 8. The variations of the mean concentration of Cl (ppm) in the Left Ravandi Aquifer (LRA) and in the Right Ravandi Aquifer (RRA) and the reservoir (R) versus the reservoir water level (RWL).

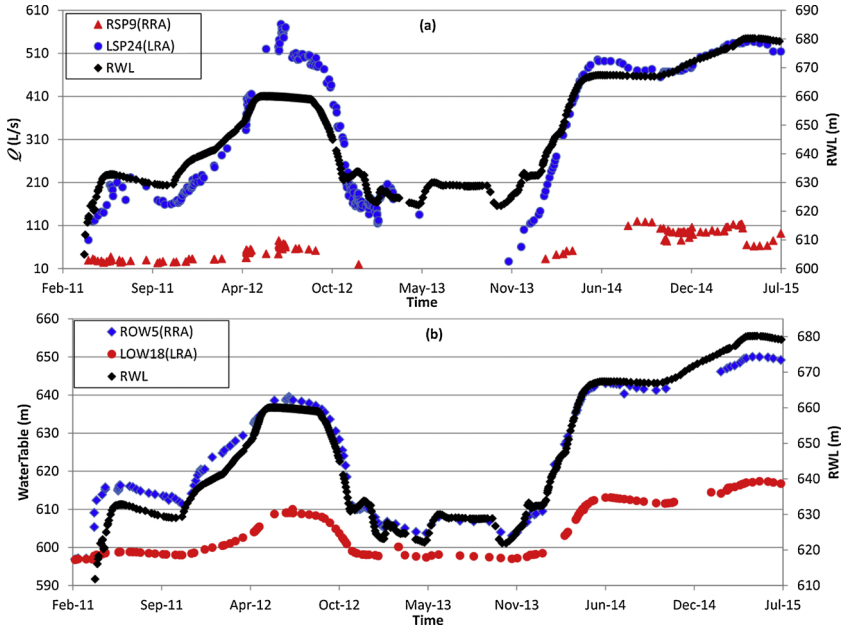

Fig. 9. The variations of a) springs discharge (RSP9 AND LSP24) and b) water table of the observation wells (ROW5 and LOW18) in the Right Ravandi Aquifer (RRA) and Left Ravandi Aquifer (LRA) versus the reservoir water level (RWL).

H and $\delta^{18}O$ in response to variation of the reservoir water level are utilized. The variations of the average Cl concentration of LRA and RRA versus the reservoir water level (RWL) are presented in Fig. 8. In general, the average Cl concentration under the post-reservoir conditions is greater than that of the pre-reservoir conditions (Fig. 8). Moreover, the average concentration of Cl in LRA and RRA increases with increasing the reservoir water level. However, the concentration of Cl in the reservoir water is less than that of the aquifers. Alternatively, water level in the aquifers and discharge of the springs increased in response to increasing reservoir water level and possible leakage to the LRA and RRA (Fig. 9). The Pearson correlation coefficient between the reservoir water level and the four sampling sites in Fig. 9 including SPR9 (RRA), LSP24 (LRA), ROW5 (RRA) and LOW18 (LRA) is 0.85, 0.93, 0.91 and 0.85, respectively. It can be deduced that halite is probably dissolved by the leakage water from the reservoir before recharging to the aquifers (Figs. 3 and 4).

Average δ^{18} O and δ^{2} H for the water samples from RRA, LRA, and GFA under pre-reservoir condition were measured -4.70‰ and -22.6; -5.25‰ and -26‰; and -4.29‰ and -24‰, respectively. Under post-reservoir condition, the average isotopic composition of RRA and LRA is -4.37‰ and -22.37‰; -4.38‰ and -23.2‰ , respectively. Meanwhile, δ^{18} O and δ^{2} H of the samples from the reservoir measured to be -2.58‰ and -15.23‰, respectively. The isotopic composition of the RRA and LRA reveal a degree of enrichment from pre-reservoir to post-reservoir conditions (Fig. 10). Average enrichment of δ^{18} O and δ^{2} H for the water samples from RRA and LRA aquifers is 0.33‰ and 0.23‰; 0.87‰ and 2.80‰, respectively. Moreover, the isotopic composition of the samples from RRA and LRA move closer to GFA under post-reservoir conditions (Fig. 10). Because of the effect of the reservoir as a high hydraulic force, it seems that the spring's water from the LRA is partly fed by GFA which cause an enrichment of the isotopic content. Therefore, the discharge of left springs may be a mixture of at least three end-members which are LRA, R and GFA. Taking the regional groundwater flow direction into account it is likely that R and GFA, at least to some extent, firstly mixed and then flow toward the springs emerge from LRA.

Comparing of isotopic content and concentration of Cl under two different hydraulic conditions reveal that the reservoir must be included in the list of end-members under post-reservoir condition. When the differences between concentrations of the major ions are not considerable and a few numbers of the conservative species are available, as in this study, the reliable number of end members should be identified using simultaneous application of EMMA and additional using of isotopic, hydrochemical and hydrogeological data together.

3.3. Mixing modeling

3.3.1. Conceptual mixing model

The MIX code was utilized for calculating the mixing ratio of the end-members. EMMA was applied with eight measured species (i.e.,Cl^{-}, SO_4^{2-}, HCO_3^{-}, K^{+}, Na^{+}, Ca^{2+}, Mg^{2+}, and EC). The reliable conceptual mixing model is assessed by evolution of considering three, four and five end-members. Since the results of EMMA suggested at least three end-members including RRA, LRA, and GF in the study area, these aquifers were selected as the end-members for the mixing modeling of the first scenario. In the second scenario, four end-members including RRA, LRA, DG, and GFA were selected to run the mixing model. The third scenario consisted of five end-members RRA, LRA, GFA, R, and DG as the end-members. The species composition of five possible end-members has been shown in Table 1. All of the models include 29 sampling sites with the 8 measured species. Since the eight species characterize the samples and the end-members together, all of them are used in the models. However the effect of applying one fewer species by turn is discussed in Section 3.3.4.

In order to evaluate the reliability of the scenarios, R^2 is used as a measure of similarity between the measured and estimated concentration of the species. Moreover, the Akaike Information Criterion (AIC), a rigorous approach for selecting a reliable model which basically prevents both underfitting and overfitting (Burnham and Anderson, 2002), was calculated for the mixing models. The relationship between the estimated and measured concentrations is assessed initially for the conservative species (i.e. Cl), then for the

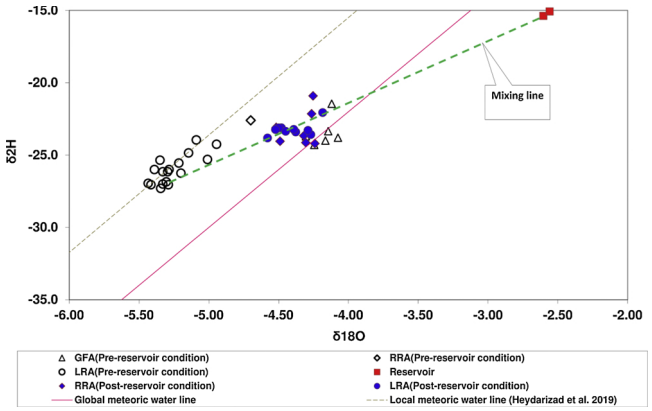

Fig. 10. Isotopic composition of the samples from the aquifers under pre-reservoir and post-reservoir conditions (RRA: right Ravandi aquifer, LRA: left Ravandi aquifer, and GFA: Gachsaran formation aquifer) (Heydarizad et al., 2019).

Table 1
The chemical composition of the species for the five end-members (R: reservoir, RRA: right Ravandi aquifer, LRA: left Ravandi aquifer, GFA: Gachsaran formation aquifer, and DG: deep groundwater).

End-member	HCO_3^-(ppm)	Cl^-(ppm)	SO_4^{2-}(ppm)	Na^+(ppm)	Mg^{2+}(ppm)	Ca^{2+}(ppm)	K^+(ppm)	EC(μs/cm)
R	191	33	305	26	24	134	3	826
RRA	156	27	301	27	26	133	3	837
LRA	198	711	397	508	36	168	3	3250
GFA	198	35	1750	23	164	540	4	2432
DG	142	46	143	54	12	45	21	551

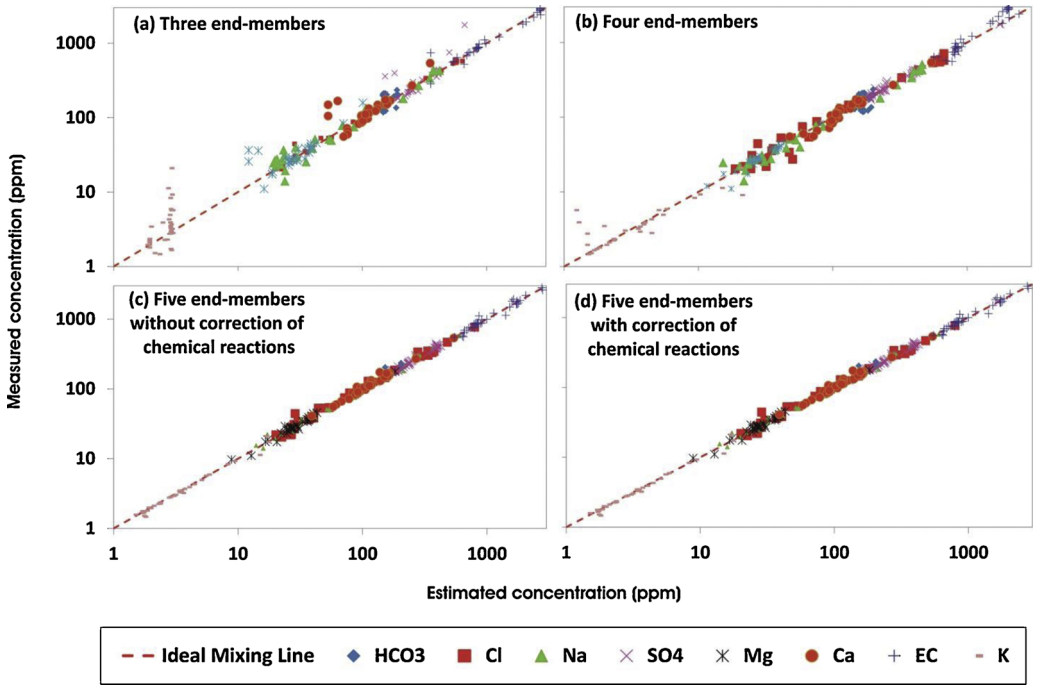

Fig. 11. Estimated versus measured concentration of major ions and EC, (a) three (LRA, RRA, and GFA), (b) four (LRA, RRA, GFA, and DG), (c) five (LRA, RRA, GFA, DG, and R without correction of chemical reactions), and (d) five (LRA, RRA, GFA, DG, and R with correction of chemical reactions) end-members scenarios (LRA: Left Ranandi Aquifer, RRA: Right Ravandi Aquifer, GFA: Gachsaran Formation Aquifers, DG: Deep Groundwater, and R: Reservoir).

rest of the species (Fig. 11). The standard deviation was assumed to be 0.10 for the conservative species (i.e. Cl, Na, EC) and 0.25 for the rest. But when the standard deviation was presumed to be 0.25 for all the species, R^2 was better, which is discussed in details in section 3.3.4. The conceptual mixing model of the five end-members was selected as the most reliable model based on the higher value of R^2 and lower value of AIC discussed in details in section 3.3.2. Therefore, in the case of the five end-members, the mass balance equation for a conservative ion C (e.g. Cl) with an inflow or outflow rate of Q in the study site can be written as:

$$C_R Q_R + C_{RRA} Q_{RRA} + C_{LRA} Q_{LRA} + C_{DG} Q_{DG} + C_{GFA} Q_{GFA} = C_S Q_S \quad (8)$$

where R, RRA, LRA, DG, GFA, and S are abbreviations for the reservoir, right Ravandi aquifer, left Ravandi aquifer, deep

Table 2
The chemical composition of the species for the five end-members after correction of the plausible chemical reactions (R: reservoir, RRA: right Ravandi aquifer, LRA: left Ravandi aquifer, GFA: Gachsaran formation aquifer, and DG: deep groundwater).

End-member	HCO_3^-(ppm)	Cl^-(ppm)	SO_4^{2-}(ppm)	Na^+(ppm)	Mg^{2+}(ppm)	Ca^{2+}(ppm)	K^+(ppm)	EC(μs/cm)
R	220	20	244	25	30	126	1	884
RRA	115	26	193	14	22	83	2	660
LRA	192	794	425	600	33	158	2	2756
GFA	158	37	1654	22	182	540	3	2796
DG	144	28	125	40	9	39	17	549

groundwater, Gachsaran formation, and mixed samples, respectively.

3.3.2. Calibration of the mixing model

Two mixing models of the five end-member scenario were run with and without correction of the plausible chemical reactions based on Eq. (7).

Despite R^2 was 0.62, 0.90, 0.95, 0.97, 0.98, 0.99, 0.99, and 0.99 for HCO_3, K, EC, Ca, SO_4, Na, Cl, and Mg, respectively, the results of the mixing model without correction of the plausible chemical reactions manifest two issues. First, the estimated concentration of HCO_3 exhibited a low correlation with the measured concentrations (R^2 = 0.62) through the calibration process. Secondly, in contrast to the results of the dye tracer tests (Behrouj et al., 2018), the mixing model shows no contribution from the reservoir at the springs emerging from LRA, such as LSP24. Moreover, the discharge of these springs and concentration of Na and Cl increased in response to the increasing of the reservoir level (Fig. 8). The mean concentration of Cl was measured in the reservoir water (30 ppm) to be less than that of the left springs emerging from LRA aquifer (575 ppm). It seems that halite dissolution is plausible as a result of movement of water from the reservoir to these springs. In order to resolve these drawbacks caused by chemical reactions, the mixing model has been run after correction of the species concentration by deduction of the effect of the plausible chemical reactions.

The results of such modified model reveal that the correlation between the measured and estimated concentration for almost all the species is improved specifically for HCO_3 which its R^2 increased from 0.62 to 0.89. The natural logarithm of the residual sum of squares (RSS) using regression model was 14.45, 14.46, 14.07, and 13 for the three end-members, four end-members, five end-members mixing model without and with the correction of plausible chemical reactions, respectively. However, AIC was 478, 493, 494, and 457 for the three end-members, four end-members, five end-members mixing model without and with the correction of plausible chemical reactions, respectively. Since the smallest AIC is an indication of the reliable model, the mixing model with the correction of the plausible chemical reaction has been selected for calculation of the mixing ratios of the end-members. Recalculations of the end-members composition are shown in Table 2. The mixing ratio of the end- members in the sampling points is presented in Fig. 12. The ratio of GFA has almost the least ratio in all the sites except in LOW13 with a ratio of 0.394. Since GF is mainly comprised of marl and gypsum, it has no significant groundwater storage which contributes in the mixed sampling points.

The ratio of DG is also low except in a few deep boreholes such as GL3B17 (0.953), foundation site (0.837), GR3B23 (0.486) and LOW9 (0.407). However, RRA aquifer extensively contributed in the right observation wells (i.e. ROWs). The mixing ratio of LRA aquifer is estimated to be from 0.40 to 0.45 for all the left springs (i.e. springs with abbreviation of LSP). In Fig. 12 the mixing ratio of the reservoir, which is in fact the value of leakage, has been illustrated. The maximum contribution of the reservoir is estimated in the drainage boreholes such as GR4B49 (0.89) and GL4B33 (0.80) which can be spotted as plausible weak zones in the dam grout curtain. Moreover, the mixing ratio of the reservoir in the springs varies from minimum of 0.40 in RSP1 to maximum of 0.64 in RSP8. The estimated mixing ratio for LSP24 the spring with flow rate of 514 L/s reveals about half of discharging water of this spring comes from the reservoir. Lack of the contribution of the reservoir in GL3B17, which is very close to the dam body, shows there are no flow paths from the reservoir toward this sampling point (Fig. 12). The results of the second mixing model (i.e. considering chemical reactions) are consistent with the geological setting (e.g. low groundwater storage of GFA), hydrogeological data (e.g. different flow system through LRA and RRA aquifers), and the previous dye tracer results (e.g. low and high contribution of the reservoir in GL3B17

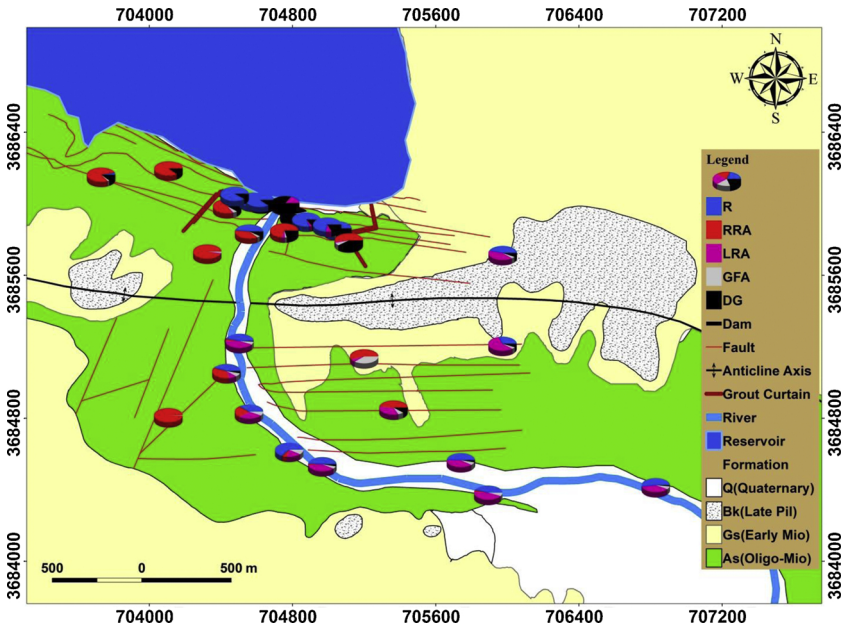

Fig. 12. The spatial distribution of the reservoir (R) mixing ratio showing contribution of leakage from the reservoir in the sampling points (RRA: Right Ravandi Aquifer, LRA: Left Ravandi Aquifer, GFA: Gachsaran Formation Aquifer, and DG: Deep Groundwater).

Table 3
The mixing ratio of the end-members in LSP24 assuming different values for SD (R: reservoir, RRA: right Ravandi aquifer, LRA: left Ravandi aquifer, GFA: Gachsaran formation aquifer, and DG: deep groundwater).

SD	DG	GFA	RRA	LRA	R
All species = 0.35	0.01	0.13	0.41	0.45	0.00
All species =0.30	0.01	0.06	0.02	0.46	0.45
All species =0.25	0.04	0.06	0.00	0.41	0.50
All species = 0.15	0.05	0.07	0.00	0.43	0.46
Cl, Na, EC = 0.1; Ca, Mg, HCO_3, SO_4, K = 0.25	0.02	0.07	0.20	0.47	0.25

and LSP24, respectively) (Behrouj et al., 2018). Accordingly, the five end-members mixing model with correction of the chemical reactions is reliable for applying in the different hydrogeological conditions in the study area.

3.3.3. Validation of the mixing model

In order to validate the mixing model (five end-members with correction of the chemical reactions), the measured data in August 2014 and September 2015 are used. The effect of reactions is corrected based on Eq. (7). The results show an acceptable level of correlation between the measured and estimated concentration as R^2 in August 2014 and September 2015 for Cl and EC is 0.99, 0.95 and 0.93, 0.88, respectively. Moreover, the mixing ratio of the reservoir in LSP24 is estimated to be 0.55 (August 2014) and 0.46 (September 2015) which are close to the ratio estimated by the calibrated mixing model for July 2015 (0.50). The maximum difference between the calculated reservoir mixing ratios in the three set of modeling (August 2014; July 2015; September 2015) for LSP24 is about 26 L/s of 514 L/s which is not much considering that the discharge of LSP24 can change due to the contribution of the other end-members in time.

3.3.4. Uncertainty of the mixing model

The known sources of uncertainty in the mixing model are the chemical reactions, the assigned standard deviation (SD) to the concentration of species and the possibility of different combinations of species used in the mixing model (Tubau et al., 2014). The final validated mixing model (five end-members with correction of the chemical reactions) and LSP24 spring are selected as the reference model, and a representative site for assessing the uncertainty of the results of the mixing model, respectively. The mixing ratios of the end-members in LSP24 and R^2 are used as the criteria of the models reliability.

The reference mixing model was run under assigning different values of SD to the species. Applied SDs were the same for all the species except for one with an SD (Cl, Na, EC) = 0.1 the rest of the species (i.e., Ca, Mg, HCO_3, SO_4, K) had an SD = 0.25. The mixing ratio of the end-members in LSP24 is shown in Table 3. The R^2 for all the models does not differ too much except for HCO_3 that had low values 0.54 and 0.73 when SD (Cl, Na, EC) = 0.1 and SD = 0.35, respectively. The average flow rate of LSP24 is 432 L/s, and ranged from 100 to 537 L/s when the reservoir water level was 633 and 680 masl, respectively. It is likely that about half of LSP24 flow rate is fed by the reservoir. Accordingly, if a mixing model estimates the reservoir mixing ratio close to 0.50 at LSP24 spring, that mixing model is reliable. Interestingly the results elucidated that the reservoir mixing ratio estimated close to 0.5 at LSP24 spring only assuming a range of 0.15 to 0.3 for SD. Hence, the other alternatives, whether SDs more than 0.30 or less than 0.15, should not be used in the mixing model.

The final validated mixing model was run several times by removing one species in turn. The R^2 value for all estimated values versus the measured values for all the models was about 0.985 for the model with five end-members with correction to the chemical reactions. The mixing ratio of the end-members in LSP24 has been changed in response to elimination of each species (Table 4). The results reveal that by removing of Cl and Mg from the set of species, the mixing ratio of the end-members in LSP24 is the same as the reference model. However, by removing the other species the mixing ratio of LSP24 was not consistent with the conceptual model because the mixing ratio of the reservoir in LSP24 was less than 0.10.

Table 4
The mixing ratio of the end-members in LSP24 in response to removal of the species through mixing modeling (R: reservoir, RRA: right Ravandi aquifer, LRA: left Ravandi aquifer, GFA: Gachsaran formation aquifer, and DG: deep groundwater).

Removed species	DG	GFA	RRA	LRA	R
Mg	0.02	0.06	0.00	0.42	0.50
Cl	0.02	0.05	0.00	0.44	0.49
SO_4	0.00	0.08	0.38	0.47	0.07
Ca	0.00	0.07	0.47	0.46	0.00
HCO_3	0.03	0.07	0.46	0.45	0.00
EC	0.01	0.07	0.45	0.47	0.00

4. Conclusion

The mixing process in a karst aquifer is modeled using the MIX code under both pre-reservoir and post-reservoir conditions. The hydrogeology and hydrochemistry of the study area were changed due to impoundment of the Seymareh reservoir as a constant head boundary with an elevation of 680 masl. The conventional statistical approaches (i.e. matrix and loading plots) are used to characterize the sampling points. Applying EMMA approach showed four end-members including the GFA, RRA, LRA aquifers, and a deep groundwater source having contribution in the discharge of the downstream springs. However, the comparison of chemical and isotopic content of water samples under pre-reservoir and post-reservoir conditions proves that the dam reservoir as the fifth end-member has a considerable effect on chemical and isotopic contentment of the downstream springs. Moreover, the conceptual model of mixing processes including five end-members was selected due to the higher R^2 between the measured and estimated concentration of the species and lower AIC in comparison to three and four end-members. The conceptual mixing model is calibrated based on considering or neglecting a few known chemical reactions. Applying this model, it was possible to quantify the leakage of the dam reservoir by calculation of its mixing ratio at different sampling sites and also to detect the weak zones of the grout curtain. The reservoir mixing ratio ranged from zero at the sampling sites very close to the dam body to about 0.50 at most springs and 0.80 at some drainage boreholes away from the dam body. The calculated ratio for the contribution of the reservoir was consistent with the results of the previous dye tracing tests and the correlation between the time variation of the reservoir water level and discharge of the springs. The employed approach is recommended to be applied in sites with different hydrogeological conditions particularly at dam sites.

Declaration of Competing Interest

The authors certify that they have no affiliations with or involvement in any organization or entity with any financial interest or non-financial interest in the subject matter or materials discussed in this manuscript.

Acknowledgments

The authors express their gratitude to the two anonymous reviewers for their constructive comments and suggestions which have contributed to improvements of the original version of the manuscript. The authors would like to thanks Shiraz University for continuous support during the field work and collection of data. This research also partly supported by Iran Water and Power Resources Development Company (IWPCO), Iran.

Appendix A. Supplementary data

Supplementary material related to this article can be found, in the online version, at doi:https://doi.org/10.1016/j.ejrh.2020.100693.

References

Bagheri, R., Raeisi, E., Zare, M., Mohammadi, Z., 2006. Leakage Potential in Seymareh Dam Site, the 26th Congress of Earth Sciences 1 Geological Mine Exploration Organization, Iran, 77e86.
Battaglia, D., Birindelli, F., Rinaldi, M., Vettraino, E., Bezzi, A., 2016. Fluorescent tracer tests for detection of dam leakages: the case of the Bumbuna dam-Sierra Leone. Eng. Geol. 205, 30–39.
Behrouj, A., 2018. Comparison of Hydrogeological and Hydrochemical Conditions in a Karst Terrain Under Low and High Gradient Flow Regimes, Seymareh Dam, Iran. Ph.D. thesis. Shiraz University.
Behrouj, A., Mohammadi, Z., Raeisi, E., Solgi, K., Mosavi, M.J., Kamali, M., 2018. Hydrogeological characterization of flow system in a karstic aquifer, Seymareh dam, Iran. J. Afr. Earth Sci. 143, 266–277.
Boleve, A., Janod, F., Revil, A., Lafon, A., Fry, J.J., 2011. Localization and quantification of leakages in dams using time-lapse self-potential measurements associated with salt tracer injection. J. Hydrol. (Amst.) 403 (3-4), 242–252.
Burnham, K.P., Anderson, D.R., 2002. A practical information-theoretic approach. Model Selection and Multimodel Inference, 2nd ed. Springer, New York.
Carrera, J., Vázquez-Suñé, E., Castillo, O., Sánchez-Vila, X., 2004. A methodology to compute mixing ratios with uncertain end-members. Water Resour. Res. 40 (12).
Chen, L., Yin, X., Xie, W., Feng, X., 2014. Calculating groundwater mixing ratios in groundwater-inrushing aquifers based on environmental stable isotopes (D, 18 O) and hydrogeochemistry. Nat. Hazards 71 (1), 937–953.
Cheshomi, A., Sahbaniya, Y., Ashjari, J., 2014. Assessment of water leakage through the right abutment of the Seymareh dam. Geopersia 4 (2), 213–225.
Christophersen, N., Hooper, R.P., 1992. Multivariate analysis of stream water chemical data: the use of principal components analysis for the end-member mixing problem. Water Resour. Res. 28 (1), 99–107.
Christophersen, N., Neal, C., Hooper, R.P., Vogt, R.D., Andersen, S., 1990. Modelling streamwater chemistry as a mixture of soilwater end-members – a step towards second-generation acidification models. J. Hydrol. (Amst.) 116, 307–320.
Contreras, I., Hernandez, S., 2013. Techniques for Prevention and Detection of Leakage in Dams and Reservoirs.
Crandall, C.A., Katz, B.G., Hirten, J.J., 1999. Hydrochemical evidence for mixing of river water and groundwater during high-flow conditions, lower Suwannee River basin, Florida, USA. Hydrogeol. J. 7 (5), 454–467.
De Simoni, M., Sanchez-Vila, X., Carrera, J., Saaltink, M.W., 2007. A mixing ratios-based formulation for multicomponent reactive transport. Water Resour. Res. 43 (7).
Douglas, M., Clark, I.D., Raven, K., Bottomley, D., 2000. Groundwater mixing dynamics at a Canadian Shield mine. J. Hydrol. (Amst.) 235 (1-2), 88–103.
Gu, H., Ma, F., Guo, J., Li, K., Lu, R., 2017. Assessment of water sources and mixing of groundwater in a coastal mine: the Sanshandao gold mine, China. Mine Water Environ. 1–15.
Hartmann, A., Goldscheider, N., Wagener, T., Lange, J., Weiler, M., 2014. Karst water resources in a changing world: review of hydrological modeling approaches. Rev. Geophys. 52 (3), 218–242.

Heydarizad, M., Raeisi, E., Sorí, R., Gimeno, L., 2019. Developing meteoric water lines for Iran based on air masses and moisture sources. Water 11 (11), 2359.
Hooper, R.P., 2003. Diagnostic tools for mixing models of stream water chemistry. Water Resour. Res. 39 (3).
Hooper, R.P., Christophersen, N., Peters, N.E., 1990. Modelling streamwater chemistry as a mixture of soil water end-members—an application to the Panola Mountain catchment, Georgia, USA. J. Hydrol. (Amst.) 116 (1-4), 321–343.
James, A.L., Roulet, N.T., 2006. Investigating the applicability of end-member mixing analysis (EMMA) across scale: a study of eight small, nested catchments in a temperate forested watershed. Water Resour. Res. 42 (8).
Joerin, C., Beven, K.J., Iorgulescu, I., Musy, A., 2002. Uncertainty in hydrograph separations based on geochemical mixing models. J. Hydrol. (Amst.) 255 (1-4), 90–106.
Jurado, A., Vázquez-Suñé, E., Carrera, J., Tubau, I., Pujades, E., 2015. Quantifying chemical reactions by using mixing analysis. Sci. Total Environ. 502, 448–456.
Jurgens, B.C., Bexfield, L.M., Eberts, S.M., 2014. A Ternary age-mixing model to explain contaminant occurrence in a deep supply well. Groundwater 52 (S1), 25–39.
Kamble, R.K., Muralidhar, B., Hanumanthappa, M.S., Patil, A.V., Edlabadkar, J.S., 2014. Multiple approaches to analyse and control seepage in hydraulic structures. ISH J. Hydraul. Eng. 20 (1), 7–13.
Katsuyama, M., Ohte, N., Kobashi, S., 2001. A three-component end-member analysis of streamwater hydrochemistry in a small Japanese forested headwater catchment. Hydrol. Process. 15 (2), 249–260.
Long, A.J., Valder, J.F., 2011. Multivariate analyses with end-member mixing to characterize groundwater flow: wind Cave and associated aquifers. J. Hydrol. (Amst.) 409 (1-2), 315–327.
Milanovic, P., 2018. Engineering Karstology of Dams and Reservoirs. CRC Press.
Mohammadi, Z., 2009. Assessing hydrochemical evolution of groundwater in limestone terrain via principal component analysis. Environ. Earth Sci. 59 (2), 429–439.
Mohammadi, Z., Raeisi, E., Bakalowicz, M., 2007a. Method of leakage study at the karst dam site. A case study: Khersan 3 Dam, Iran. Environ. Geol. 52 (6), 1053–1065.
Mohammadi, Z., Raeisi, E., Zare, M., 2007b. A dye-tracing test as an aid to studying karst development at an artesian limestone sub-aquifer: Zagros Zone, Iran. Environ. Geol. 52 (3), 587–594.
Nakaya, S., Uesugi, K., Motodate, Y., Ohmiya, I., Komiya, H., Masuda, H., Kusakabe, M., 2007. Spatial separation of groundwater flow paths from a multi-flow system by a simple mixing model using stable isotopes of oxygen and hydrogen as natural tracers. Water Resour. Res. 43 (9).
Pelizardi, F., Bea, S.A., Carrera, J., Vives, L., 2017. Identifying geochemical processes using End Member Mixing Analysis to decouple chemical components for mixing ratio calculations. J. Hydrol. (Amst.) 550, 144–156.
Raeisi, E., Kowsar, N., 1997. Development of Shahpour Cave, southern Iran. Cave Karst Sci. 24 (1), 27–34.
Ravenscroft, P., McArthur, J.M., 2004. Mechanism of regional enrichment of groundwater by boron: the examples of Bangladesh and Michigan, USA. Appl. Geochem. 19 (9), 1413–1430.
Rueedi, J., Purtschert, R., Beyerle, U., Alberich, C., Kipfer, R., 2005. Estimating groundwater mixing ratios and their uncertainties using a statistical multi parameter approach. J. Hydrol. (Amst.) 305 (1-4), 1–14.
Scheiber, L., Ayora, C., Vázquez-Suñé, E., 2018. Quantification of proportions of different water sources in a mining operation. Sci. Total Environ. 619, 587–599.
Sun, L., Gui, H., 2015. Hydro-chemical evolution of groundwater and mixing between aquifers: a statistical approach based on major ions. Appl. Water Sci. 5 (1), 97–104.
Tubau, I., Vàzquez-Suñé, E., Jurado, A., Carrera, J., 2014. Using EMMA and MIX analysis to assess mixing ratios and to identify hydrochemical reactions in groundwater. Sci. Total Environ. 470, 1120–1131.
Valder, J.F., Long, A.J., Davis, A.D., Kenner, S.J., 2012. Multivariate statistical approach to estimate mixing proportions for unknown end members. J. Hydrol. (Amst.) 460, 65–76.
Vázquez-Suñé, E., Carrera, J., Tubau, I., Sánchez-Vila, X., Soler, A., 2010. An approach to identify urban groundwater recharge. Hydrol. Earth Syst. Sci. 14 (10), 2085–2097.